Electronic Supplementary Information (ESI†)

A strategically designed porous iron/iron oxide matrix on graphene for heavy metal adsorptions

Prasenjit Bhunia, Giyoun Kim, Chul Baik and Hyoyoung Lee*

National Creative Research Initiative, Center for Smart Molecular Memory, Department of Chemistry, Sungkyunkwan University, 300 Cheoncheon-dong, Jangan-gu, Suwon, Gyeonggi-do 440-746, Korea.

E-mail: hyoyoung@skku.edu

1. Materials and Methods

A. Chemicals

Natural graphite (Bay Carbon, SP-1 graphite), sulfuric acid (95-97%) (OCI Company Ltd.), hydrogen peroxide (30 wt.%) (OCI Company Ltd.), potassium permanganate (99.3%) (Samchun Pure Chemical Co. Ltd.), sodium nitrate (97%) (Sigma-Aldrich.), were obtained from commercial sources. Sodium borohydride (98% Sigma-Aldrich) ferrous chloride tetrahydrate (98% Fluka), ferric chloride hexahydrate (97% Sigma-Aldrich) and ferric nitrate nonahydrate (99% Sigma-Aldrich) were obtained from Aldrich and used as received. Unless otherwise stated, other reagents were of analytical grade and were used as received.

B. Instruments

Raman spectroscopy measurements were taken using a micro-Raman system (Renishaw, RM1000-inVia) with an excitation energy of 2.41 eV (514 nm). FT-IR spectra were collected using a Thermo Nicolet AVATAR 320 instrument. Powder XRD patterns were recorded on a D8 ADVANCE instrument using Cu-Kα radiation. The superparamagnetic behavior was characterized by a Quantum Design MPMS XL (with a SQUID detector). Mössbauer spectra were recorded at room temperature with a 50 mCi 57Co source in an Rh matrix. The spectrometer was calibrated by collecting the Mössbauer spectra of a standard Fe foil at room temperature. BET surface area was measured by BELSORP-mini II. To detect the concentrations of toxic elements in water, ICP-OES was carried out using a Varian 720-ES.

C. Preparation of graphene oxide

Graphene oxide (GO) was prepared from natural graphite powder by the modified Hummers and Offenman's method using sulphuric acid, potassium permanganate, and sodium nitrate.[1]

D. Preparation of rGO-Fe_3O_4, rGO-Fe(0)/Fe_3O_4 and rGO-Fe(0):

In a round-bottomed flask, 50 mL of a 1 M solution of $FeCl_3$, $6H_2O$ was added to an aqueous solution of GO (1 g in 250 mL), 1 ml/min by a syringe pump under constant stirring in an inert atmosphere. The solution was stirred for 10 h in the same condition. Then, an alkaline solution (pH 10 by NaOH) of sodium borohydride (150 ml, 1.6 M) was added drop-wise (0.01 mL/min) into the slurry at 25ºC by the syringe pump. After this addition, the reaction mixture was stirred under an N_2 atmosphere for 12 h at the same temperature. After the completion of the reaction, the solution was centrifuged at 5000 rpm for 20 min to remove the excess iron salt and $NaBH_4$. The solvent was immediately changed to ethanol, and the mixture was centrifuged again at the same rpm and time. Again, the supernatant was replaced by fresh ethanol. The material in the ethanol was sonicated for 30 min and filtered through a membrane filter (0.2 μm, Whatman). The material was dried in a vacuum oven at 60°C for 12 h to yield rGO-Fe_3O_4. The rGO-Fe_3O_4 was synthesized by the same procedure using $Fe(NO_3)_3.9H_2O$ and $FeCl_2.4H_2O$ as the iron source. This solid (rGO-Fe_3O_4 prepared using different iron source) was then placed in an alumina boat in a quartz tube inside a tube furnace and heated at 400°C to get rGO-Fe(0)/Fe_3O_4 and at 600°C to get rGO-Fe(0), with a heating rate of 5°C/min, under an H_2/Ar (4%) atmosphere at a flow rate of 200 ccpm and was kept at that temperature for 2 h. The resulting materials, rGO-Fe(0) and rGO-Fe(0)/Fe_3O_4, were handled in air for characterization and other applications. The BET surface area data of the material prepared in different temperatures and different iron source were summarized in the Table S1.

When we repeated the experiment with different iron sources ($FeCl_3.6H_2O$, $FeCl_2.4H_2O$ and $Fe(NO_3)_3.9H_2O$). In all the cases, we obtained the same trend of BET relative surface area data. (Table S1). At 400ºC thermal annealing, the surface area increased and yielded a porous

structure comprised of rGO-Fe(0)/Fe_3O_4. On the other hand, the relative surface area at 600ºC reduced and yielded a less porous structure.

E. Raman Spectra

The Raman spectra (514 nm excitation) of as-made rGO-Fe_3O_4 and the samples heated at 400ºC and 600ºC clearly displayed two intense peaks at ~1335 cm^{-1} and 1600 cm^{-1}. These peaks correspond to the well-defined D and G bands, respectively (Fig. S1(a)). The G band is attributed to first-order scattering of the E_{2g} mode for sp^2 carbon domains, while the D band is associated with structural defects, amorphous carbon, or edges that break the symmetry and selection rule. With increasing disorder, the G and D bands broaden, although the D band is of relatively higher intensity than the G band. Therefore, the ratio of D to G band intensity ($r = I_D/I_G$) is used as a measure of the disorder. The intensity ratios (r) for as-made rGO-Fe_3O_4 (1.27), the sample heated at 400ºC (1.19), and the sample heated at 600ºC (1.23) (Fig. S1(a)) were larger than the intensity ratio for GO (0.91). This indicates defects within the sp^2 carbon network that arose upon reduction of the exfoliated GO. The second order Raman feature, *viz.* 2D, is very sensitive to the stacking order and number of rGO sheets along the c-axis. It can be concluded that the samples consist of highly disordered and randomly arranged rGO, leading to their dispersibilty in water. Chandra *et. al.* also reported such type of observation.[2]

F. Magnetic Measurement

The magnetic hysteresis curves were recorded at 300 K (room temperature) and 25 K for the as-made rGO-Fe_3O_4 and the samples heated at 400ºC and 600ºC, as shown in Fig. S1 (c) and (d)**.** The M-H loops show non-linear and reversible magnetic hysteresis in the as-made rGO-Fe_3O_4 and in the sample heated at 400ºC, but no hysteresis (zero coercivity) in the sample heated at

600ºC, and all of them exhibit superparamagnetic behavior.[2,3] The saturation magnetization (M_s), remanence (M_r) and coercivity for the as-made rGO-Fe_3O_4 and the samples heated at 400°C and 600°C are summarized in Table S2.

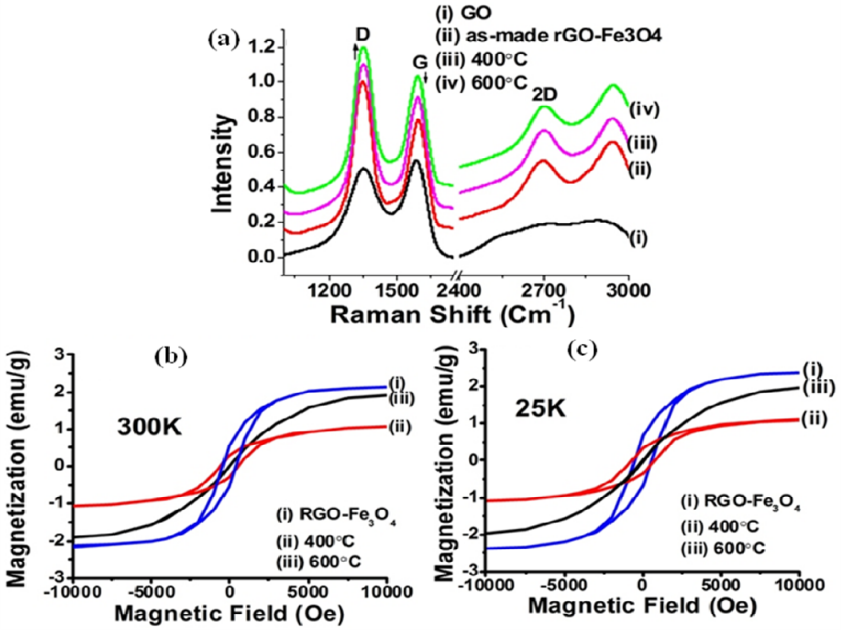

Figure S1. Raman and magnetic measurement data of the composites. (a) Raman spectra, and hysteresis curves at (b) 300 K and (c) 25 K for as-made rGO-Fe_3O_4 and samples heated at 400ºC and 600ºC.

G. TEM and HRTEM

Fig. S2 shows the TEM images of rGO-Fe_3O_4 (a), rGO-Fe(0)/Fe_3O_4 (b), rGO-Fe(0) (d). As the rGO sheets were crumpled in nature, it is difficult to tell from the TEM images whether the iron/iron oxide nanoparticles were on the outer surface of the carbon sheets or in between. The TEM images shows Fe_3O_4 and Fe(0) are well dispersed in the rGO matrix with particle size ranging from 10 to 50 nm. The Fe_3O_4 and Fe(0) nanoparticles are not simply mixed up or blended with rGO, rather, they are entraped inside the rGO sheets. Clear lattice fringes in the HRTEM images of rGO-Fe(0)/Fe_3O_4, rGO-Fe(0) (Fig. S2 c and e) indicates the formation of highly crystalline iron nanoparticles. The interplaner distance between the fringes is 0.3 nm, (Fig.

S2(c) inset) which corresponds to the (110) plane of body centered cubic (*bcc*) iron. In the reported rGO-Fe(0) the interplaner distance of the (110) plane of *bcc* iron is 0.2nm.[3] But in rGO-Fe(0)/Fe_3O_4 the interplaner distance between the fringes is higher may be due to presence of Fe_3O_4. The rGO nanosheets enjoy a privileged role to increase the robustness of Fe_3O_4 and Fe(0) nanoparticles from surface oxidation.

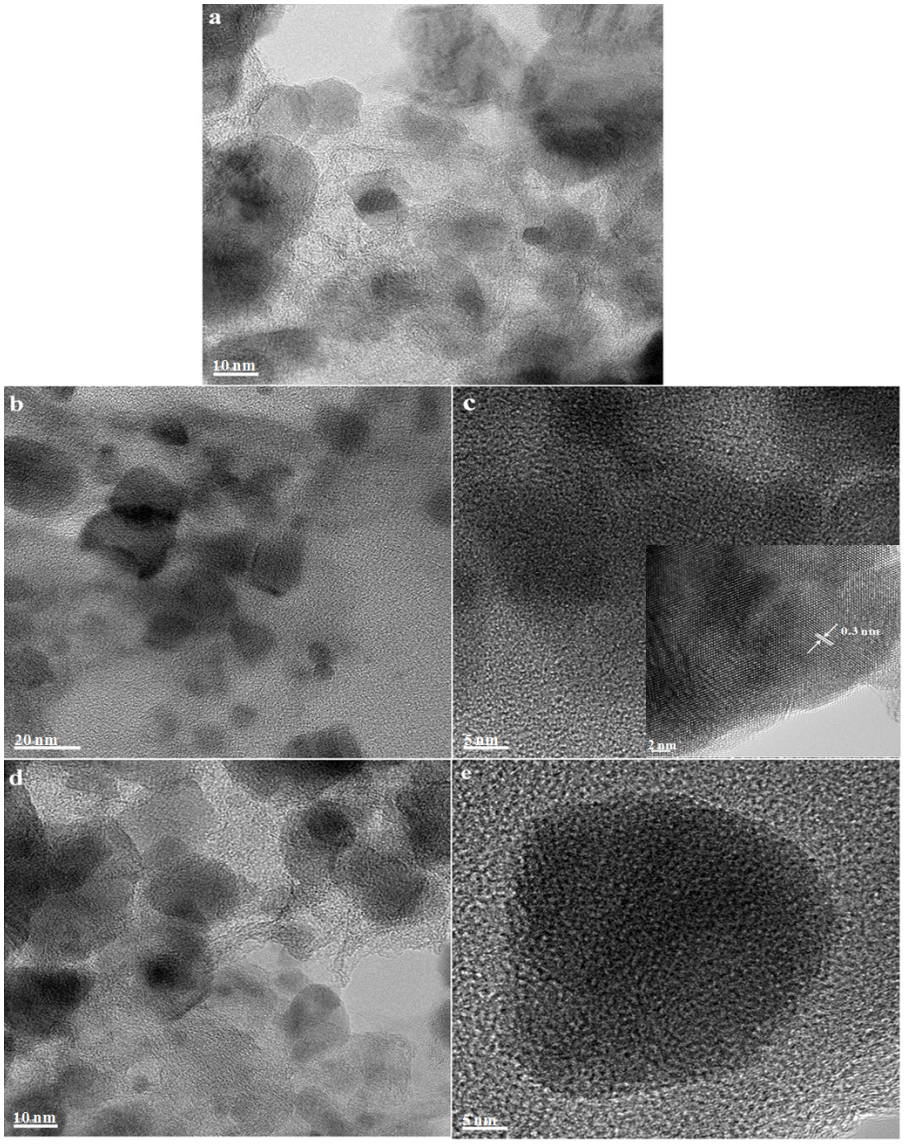

Figure S2. TEM image of rGO-Fe_3O_4 (a), rGO-Fe(0)/Fe_3O_4 (b), rGO-Fe(0) (d). HRTEM image of rGO-Fe(0)/Fe_3O_4 (c), rGO-Fe(0) (e).

Figure S3. The rGO-Fe(0)/Fe_3O_4 composite dispersed in a water solution and after magnetic separation.

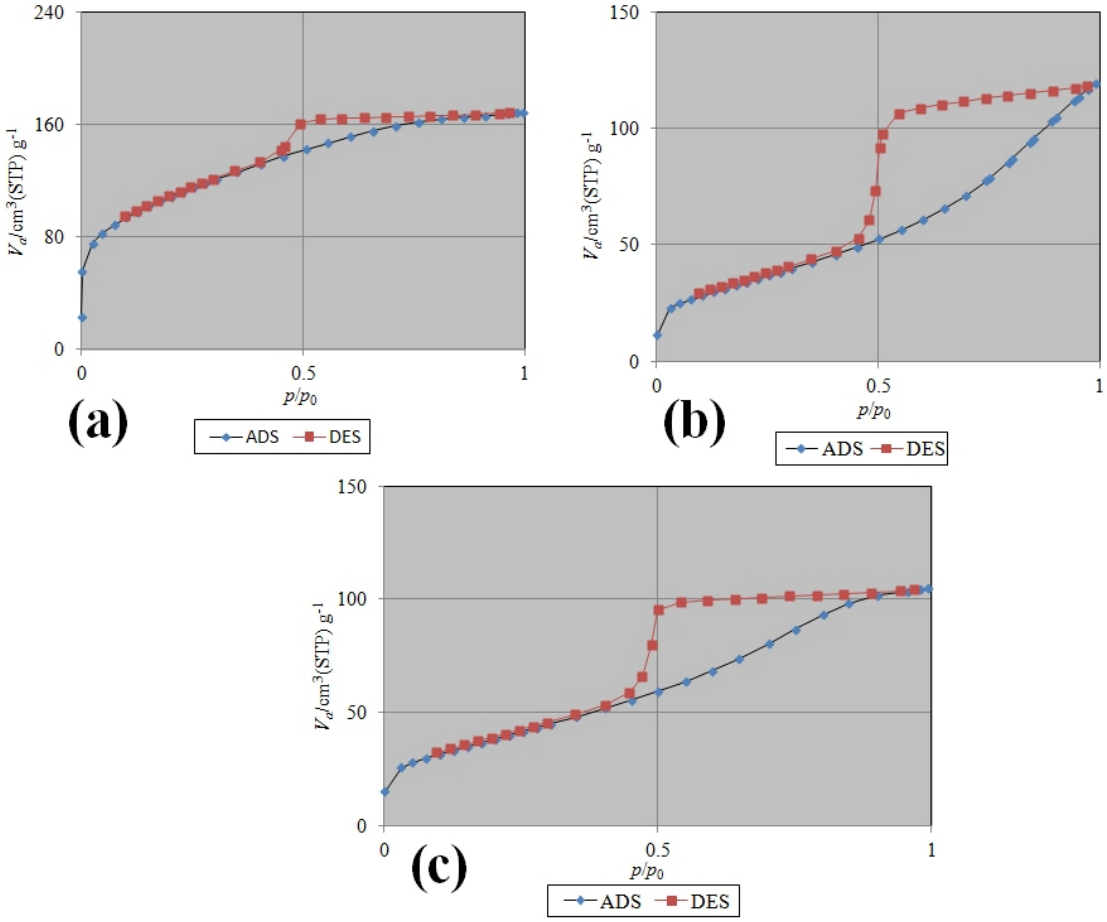

Figure S4. The Adsorption / desorption isotherm of (a) rGO-Fe(0)/Fe_3O_4 (b)) rGO-Fe(0) (c)) rGO-Fe_3O_4 composites.

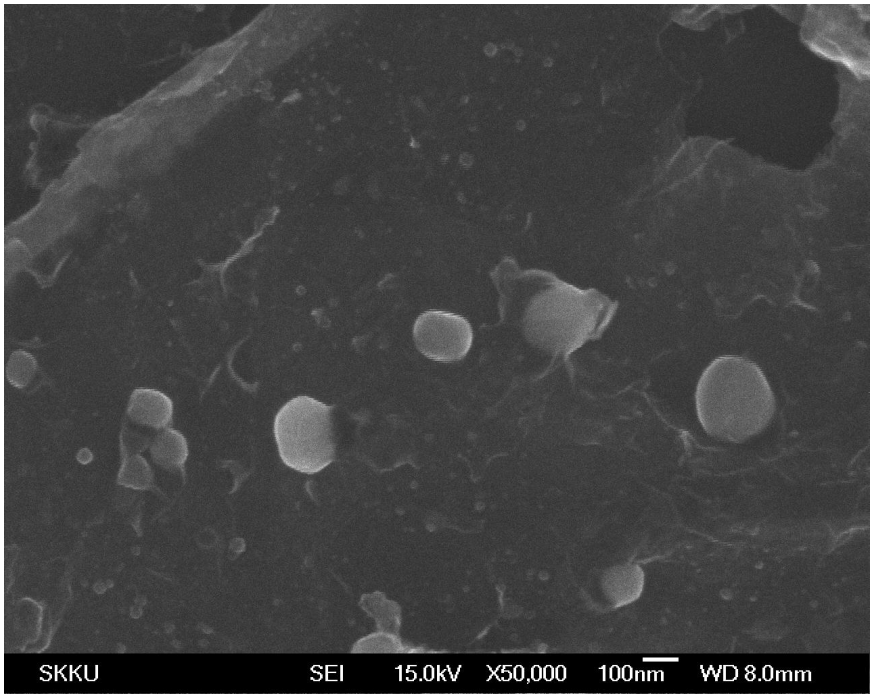

Figure S5 SEM image of SEM image of rGO-Fe(0)/Fe_3O_4

H. Heavy metal ion adsorption study:

To study the arsenic adsorption efficiency of the composite materials, a 10 ppm solution of As_2O_3 was prepared. The rGO-Fe_3O_4, rGO-Fe(0)/Fe_3O_4 and rGO-Fe(0) composites were dispersed in water (dispersibilities were 0.6, 0.5 and 0.3 mg/mL, respectively) can be separated from water with a magnet (Figure S3). In the applied field of ~20 mT, the separation was almost completed within 30 s. The composite materials were added to the 10 ppm As_2O_3 solutions in 0.5, 1, 2, and 4 mg increments by weight per 10 mL. Each solution was sonicated for 5 min and then kept standing for 55 min. Next, the composite was separated from the solutions with a magnet, and the concentration of the remaining As(III) was measured by ICP-OES. The uptake amounts of As(III) by the composite materials were calculated using the following formula:

$$Q_e = V(C_i-C_e)/(1000 \times M)$$

where Q_e is the uptake amount of As(III) on the composite materials per unit weight of the adsorbent (mg/g), C_i is the initial concentration of the As(III) solution (ppm), C_e is the equilibrium concentration (ppm), V is the volume of As(III) solution used (mL) and M is the weight of the adsorbent material used (in g).

From the data, as summarized in Fig. 2(i), it could be concluded that, at higher adsorbent concentrations, the arsenic adsorption efficiency was low. At lower adsorbent concentrations, the arsenic adsorption efficiency showed the highest adsorption due to presence of Fe(0) in the rGO-Fe(0)/Fe_3O_4 and to effective interaction with arsenate anions. The optimal arsenic removal was achieved with the porous rGO-Fe(0)/Fe_3O_4, followed by the rGO-Fe(0) and then the rGO-Fe_3O_4. As the adsorption was highest for an adsorbent concentration of 0.05 g/L, further experiments were performed at this concentration. Aqueous solutions with different initial arsenic concentrations varying from 2 to 6 ppm were used for the experiments at pH 7, adsorption time 1 h, temperature 25 °C, and adsorbent concentration 0.05 g/L, as shown in Fig. 2(ii). The data for the arsenic adsorption were fitted with the Langmuir isotherm model. Langmuir isotherm is expressed as follows:

$$Q_e = abC_e/(1+bC_e)$$

where Q_e is the amount of arsenic adsorbed per unit weight of adsorbent (mg/g), C_e is the equilibrium concentration of arsenic (mg/L), b is the constant related to the free energy of adsorption (L/mg) and a is the maximum adsorption capacity (mg/g).

A nonlinear fitting was applied to obtain all Langmuir isotherm parameters (R^2 = 0.95). The adsorption constants evaluated from the isotherms for rGO-Fe_3O_4, rGO-Fe(0)/Fe_3O_4, and rGO-Fe(0) are listed in Table S3. The maximum adsorption capacity for arsenic ions is shown in the diagram in Fig. 2(iii). The adsorption capacity of As(III) was highest in rGO-Fe(0)/Fe_3O_4 (44 mg/g), followed by that in rGO-Fe(0) (37 mg/g), and lowest in rGO-Fe_3O_4 (21 mg/g). In comparison with previously reported results for Cr(VI), a removal capacity of 162 mg/g, roughly four times that of our results for rGO-Fe(0) (37 mg/g), indicated a nearly equivalent result since the applied adsorbent concentration (0.2 g/L) and adsorption time (4 h) were also four times higher than ours,[3] indicating that our porous rGO-Fe(0)/Fe_3O_4 produced the higher adsorption capacity.

The pH-dependent behavior of the arsenic adsorption onto rGO-Fe(0)/Fe_3O_4 and rGO-Fe(0) showed the co-effects of several competing factors controlling the adsorption reaction. It was proposed that the adsorption of arsenite onto the surface of rGO-Fe(0)/Fe_3O_4 proceeds in three steps: (1) migration to the surface; (2) dissociation (or deprotonation) of complexed aqueous arsenite; (3) surface complexation. Step 1 is the prerequisite of the adsorption reaction and is largely controlled by the electrostatic attraction or repulsion of the aqueous arsenite species with the surface of the adsorbent. Hence, the pH of zero point charges (pH_{ZPC}, around pH 7.3)[4] of the adsorbent and the speciation of aqueous arsenite were the governing factors. It is well known that the solid surface of the rGO-Fe(0)/Fe_3O_4 is positively charged at any pH below pH_{ZPC} and negatively charged at any pH above pH_{ZPC}, resulting in increased electrostatic attraction or repulsion with anionic arsenic species and leading to enhanced or inhibited adsorption.[4] H_3AsO_3 is predominant at pH 4.5 to 6, a mixture of H_3AsO_3 and $H_2AsO_3^-$ at pH 6 to 8, a mixture of $H_2AsO_3^-$ and $HAsO_3^{2-}$ at pH 8 to 12, and a mixture of $HAsO_3^{2-}$ and AsO_3^{3-} at pH 12 to 14.[5]

As(III) removal was enhanced when pH increased from 4.5 to 7.3 due to the adsorption of negatively and neutrally charged arsenite on the positively charged surface of the rGO-Fe(0)/Fe_3O_4. At pH greater than 7.3, the negatively charged surface of the rGO-Fe(0)/Fe_3O_4 showed electrostatic repulsion against anionic arsenite species, which led to decreased adsorption with increasing pH. The As(III) adsorption was maximized at a pH around 7.3 (Fig. S5(a)).

The effect of temperature on arsenic adsorption is depicted in Fig. S5(b). The temperature was varied from 10 to 50°C. Arsenic adsorption increased from 10 to 30°C but decreased at higher temperatures. Higher temperatures would cause faster molecular movement, facilitating the aggregation of the nanoparticles, so the agglomerization intensified when temperature increased, and then the activity of Fe(0) decreased. At temperatures greater than 30°C, agglomeration was the dominant mechanism. Wu *et al*. also observed such behavior for Cr(VI) on Fe(0).[6]

Fig. S5(c) shows the adsorption of arsenite on rGO-Fe(0)/Fe_3O_4 and rGO-Fe(0) as a function of time. At the beginning the arsenic adsorption increased with increase of adsorption time, and then there is a saturation of arsenic adsorption may be due to the occupancy of all adsorption sites available on the adsorbent. Because of this may be the arsenic adsorption didn't increase linearly with prolongation of adsorption time.[3] The kinetic data for the sorbent were fitted to a pseudo-second-order kinetic model.[3] The kinetic rate equation is expressed as

$$dQ_t/dt = K_2(Q_e - Q_t)^2$$

where Q_e is the sorption capacity at equilibrium and Q_t is the uptake of arsenic at time t. The quantity k_2 (mL mg^{-1} min^{-1}) represents the pseudo-second-order rate constant. By integrating equation

$$t/Q_t = K_2/Q_e^2 + 1/Q_e t$$

with the boundary conditions of $Q_t = 0$ at $t = 0$ and $Q_t = Q_t$ at $t = t$, the following linear equation can be obtained:

$$V_0 = K_2 Q_e^2$$

where V_0 (mg mL^{-1} min^{-1}) is the initial sorption rate. Therefore, the V_0 and Q_e values can be determined experimentally by plotting t/Q_t versus t (Fig. S5(d)). The pseudo-second-order kinetic parameters are summarized in Table S4.

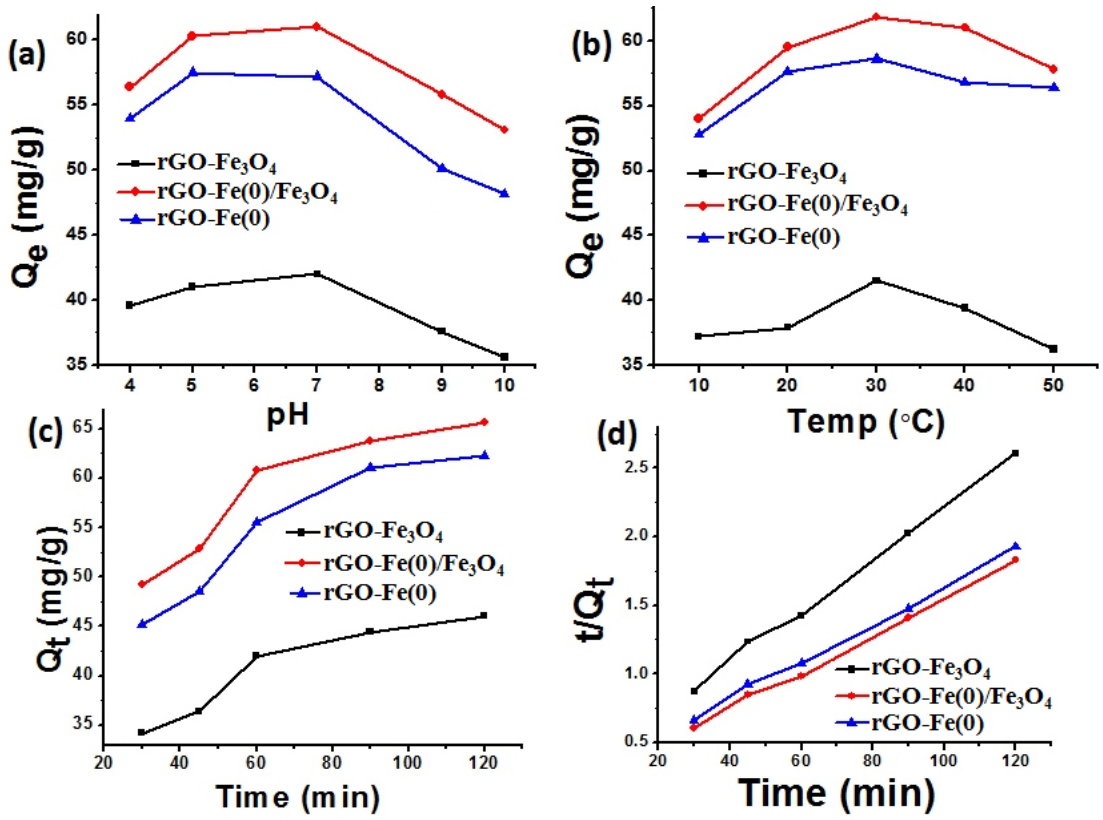

Figure S5. Influences of pH, temperature, and time on arsenic adsorption by the rGO-Fe_3O_4, rGO-Fe(0)/Fe_3O_4 and rGO-Fe(0) composite. (a) Effect of pH on arsenic adsorption: temperature, 20°C; adsorption time, 1 h; adsorbent dosage, 0.05 mg/L; arsenic concentration, 5 ppm. (b) Effect of temperature on arsenic adsorption: pH, 7; adsorption time, 1 h; adsorbent dosage, 0.05 mg/L; arsenic concentration, 5 ppm. (c) Time profile of arsenic adsorption: temperature, 20°C; pH, 7; adsorbent dosage, 0.05 mg/L; and arsenic concentration, 5 ppm on different adsorbents. (d) The transformed rate plot t/Q_t vs. t.

Table S1. BET surface area, pore volume and pore size of as made rGO-Fe_3O_4, rGO-Fe(0)/Fe_3O_4 and rGO-Fe(0).

(i) $FeCl_3.6H_2O$ as the iron source.

Sample	Surface Area (m^2/g)	Pore Volume (Cm^3/g)	Pore Size (nm)
rGO-Fe_3O_4	140.70	0.16	4.62
rGO-Fe(0)/Fe_3O_4	384.62	0.26	2.71
rGO-Fe(0)	124.34	0.18	5.92

(ii) $FeCl_2.4H_2O$ as the iron source.

Sample	Surface Area (m^2/g)	Pore Volume (Cm^3/g)	Pore Size (nm)
rGO-Fe_3O_4	44.18	0.19	1.6
rGO-Fe(0)/Fe_3O_4	73.95	0.29	2.36
rGO-Fe(0)	6.89	0.04	-

(iii) $Fe(NO_3)_3.9H_2O$ as the iron source.

Sample	Surface Area (m^2/g)	Pore Volume (Cm^3/g)	Pore Size (nm)
rGO-Fe_3O_4	83.42	0.14	7.17
rGO-Fe(0)/Fe_3O_4	208.95	0.21	4.02
rGO-Fe(0)	86.00	0.16	7.54

Table S2. Saturation Magnetization (Ms), Remanence (Mr), Coercive Field (Hc) of as made rGO-Fe_3O_4, rGO-Fe(0)/Fe_3O_4 and rGO-Fe(0) at 25 and 300K.

Samples	Temperature(K)	M_s ($emug^{-1}$)	Mr ($emug^{-1}$)	Coercivity(H_c) (Oe)
rGO-Fe_3O_4	25K	2.41	0.75	<1000
	300K	2.15	0.62	1000
rGO-Fe(0)/Fe_3O_4	25	1.15	0.37	1000
	300K	1.12	0.25	1500
rGO-Fe(0)	25K	2.04	0	0
	300K	1.95	0	0

Table S3. Langmuir Adsorption Isotherm Parameters for As(III) on rGO-Fe_3O_4, rGO-Fe_3O_4/ZVI and rGO-ZVI composites.

Isotherm type	Isotherm constants	rGO-Fe_3O_4	rGO-Fe(0)/Fe_3O_4	rGO-Fe(0)
Langmuir	a (mg/g)	21.2	44.4	37.3
	b (L/mg)	0.05	0.02	0.02

Table S4. Pseudo-second-order kinetic parameters for arsenic removal on the rGO-Fe_3O_4, rGO-Fe(0)/Fe_3O_4 and rGO-Fe(0).

Isotherm constants	rGO-Fe_3O_4 $R^2 = 0.99$	rGO-Fe(0)/Fe_3O_4 $R^2 = 0.99$	rGO-Fe(0) $R^2 = 0.99$
Q_e (mg/g)	52.91	75.18	72.99
K_2 (mL mg^{-1} min^{-1})	$1.08x10^{-3}$	$8.22x10^{-4}$	$6.98x10^{-4}$
V_0 (mg mL^{-1} min^{-1})	3.04	4.65	3.72

Table S5. Langmuir Adsorption Isotherm Parameters for As(III), Cr(VI), Hg(II), Pb(II) and Cd(II) on rGO-Fe(0)/Fe_3O_4.

Element	Langmuir Isotherm Constants	
	a (mg/g)	b (L/mg)
As(III)	44.4	0.02
Cr(VI)	31.1	0.04
Hg(II)	22.0	0.03
Pb(II)	19.7	0.04
Cd(II)	1.91	0.10

Table S6. Arsenic removal efficiency of the rGO-Fe(0)/Fe_3O_4 from natural water samples.

Sample no	Arsenic conc. (ppb)		Adsorbed conc.(Ci-Ce)	Removal efficiency (R %)
	Initial Ci	Final Ce		
1	0.98	0.11	0.87	89.4
2	1.24	0.13	1.11	90.2
3	1.45	0.14	1.31	90.5
4	3.10	0.21	2.88	93
5	4.65	0.27	4.37	94.1
6	4.82	0.27	4.54	94.3

References

1 I. K. Moon, J. Lee, R. S. Ruoff, H. Lee, *Nat. Commun*. 2010, **1**, 73.
2 V. Chandra, J. Park, Y. J. Chun, W. Lee, I. C. Hwang and K. S. Kim, *ACSnano*, 2010, **4**, 3979.
3 H. Jabeen, V. Chandra, S. J. Jung, W. Lee, K. S. Kim and S. B. Kim, *Nanoscale*, 2011, **3**, 3583.
4 H. Zhu, Y. Jia and H. X. Wua, *Journal of Hazardous Materials*, 2009, **172**, 1591.
5 K. Fields, A. Chen, L. Wang, Arsenic Removal from Drinking Water Iron Removal Plants, National Risk Management Laboratory, Office of Research and Development, US Environmental Protection Agency, Cincinnati, OH 45286. Page 2
6 Y. Wu, J. Zhang, Y. Tong and X. Xu, *Journal of Hazardous Materials,* 2009, **172**, 1640.